Inorganic Chemistry

Article

pubs.acs.org/IC

Magneto-Structural Correlations in a Series of Pseudotetrahedral $[Co^{II}(XR)_4]^{2-}$ Single Molecule Magnets: An ab Initio Ligand Field Study

Elizaveta A. Suturina,[†,‡] Dimitrios Maganas,[†] Eckhard Bill,[†] Mihail Atanasov,*[,†,§] and Frank Neese*[,†]

[†]Max Planck Institute for Chemical Energy Conversion, Stiftstrasse 34-36, D-45470 Mülheim an der Ruhr, Germany

[‡]Novosibirsk State University, Pirogova 2, 630090, Novosibirsk, Russia

[§]Institute of General and Inorganic Chemistry, Bulgarian Academy of Sciences, Akad. Georgi Bontchev Street 11, 1113 Sofia, Bulgaria

Supporting Information

ABSTRACT: Over the past several decades, tremendous efforts have been invested in finding molecules that display slow relaxation of magnetization and hence act as single-molecule magnets (SMMs). While initial research was strongly focused on polynuclear transition metal complexes, it has become increasingly evident that SMM behavior can also be displayed in relatively simple mononuclear transition metal complexes. One of the first examples of a mononuclear SMM that shows a slow relaxation of the magnetization in the absence of an external magnetic field is the cobalt(II) tetra-thiolate $[Co(SPh)_4]^{2-}$. Fascinatingly, substitution of the donor ligand atom by oxygen or selenium dramatically changes zero-field splitting (ZFS) and relaxation time. Clearly, these large variations call for an in-depth electronic structure investigation in order to develop a qualitative understanding of the observed phenomena. In this work, we present a systematic theoretical study of a whole series of complexes $(PPh_4)_2[Co(XPh)_4]$ (X = O, S, Se) using multireference ab initio methods. To this end, we employ the recently proposed ab initio ligand field theory, which allows us to translate the ab initio results into the framework of ligand field theory. Magneto-structural correlations are then developed that take into account the nature of metal−ligand covalent bonding, ligand spin−orbit coupling, and geometric distortions away from pure tetrahedral symmetry. The absolute value of zero-field splitting increases when the ligand field strength decreases across the series from O to Te. The zero-field splitting of the ground state of the hypothetical $[Co(TePh)_4]^{2-}$ complex is computed to be about twice as large as for the well-known $(PPh_4)_2[Co(SPh)_4]$ compound. It is shown that due to the π-anisotropy of the ligand donor atoms (S, Se) magneto-structural correlations in $[Co(OPh)_4]^{2-}$ complex differ from $[Co(S/SePh)_4]^{2-}$. In the case of almost isotropic OPh ligand, only variations in the first coordination sphere affect magnetic properties, but in the case of S/SePh ligand, variations in the first and second coordination sphere become equally important for magnetic properties.

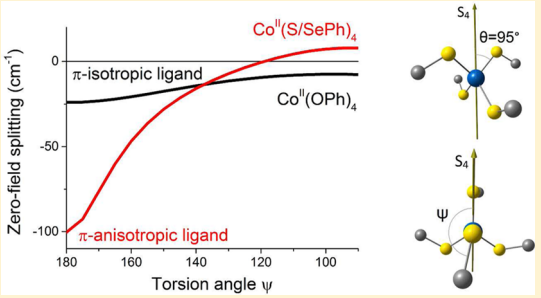

1. INTRODUCTION

Single molecule magnetism evolved as a research field at the borderline between chemistry and physics.[1,2] Similar to classical bulk magnets, single molecule magnets (SMMs) are molecules which display a large magnetic anisotropy and hence have a pronounced preferred direction of magnetization. For such molecules, below a given temperature, magnetic moments induced by an external magnetic field are preserved after switching-off the field and the magnetic moment as a function of applied field shows a pronounced hysteresis. The hysteretic behavior opens the possibility to use such SMMs as single-molecule switches. Hence, potential application of such molecules as nanoscale devices[2−4] as well as the fundamental interest in the correlation between the magnetic anisotropy[5,6] and the electronic and molecular structure are the dominant driving forces in this rapidly developing field.

The concept of SMMs was first described for an oligonuclear Mn_{12} acetato complex with a large ground state total spin $S = 10$.[7] The model put forward for the explanation of the hysteretic behavior involves the preparation of the system in the maximum magnetic sublevel $M_S = -S$. Relaxation involves stepwise transitions between the M_S levels. For a negative ZFS parameter D, the highest energy magnetic sublevel is $M_S = 0$ and the physical situation is reminiscent to a chemical reaction over a barrier. Since the height of the barrier is proportional to $|D|S^2$, very significant efforts have been undertaken to find molecules with maximal total spin S.[8−10] However, it has been pointed out that D itself is proportional to $1/S^2$, hence rendering the barrier approximately independent of S.[5,11−13] Therefore, even mononuclear complexes can exhibit SMM properties, and the first examples were lanthanides complexes.[14] Later studies on a series of mononuclear iron(II) complexes[15−18] also emphasized the effect of the large magnetic anisotropy rather than large spin for the slow relaxation of the magnetization. The anisotropy of a mononuclear transition metal complex is controlled by interplay of the ligand field and spin−orbit coupling. A prime example of a rationally designed

Received: July 28, 2015
Published: October 7, 2015

ACS Publications © 2015 American Chemical Society

DOI: 10.1021/acs.inorgchem.5b01706
Inorg. Chem. 2015, 54, 9948−9961

monomolecular SMM is a linear two-coordinated iron(I) complex with larger relaxation barrier than the classical Mn_{12}-acetato compound.[19]

Slow relaxation of the magnetization without an applied magnetic field was also described for the tetraphenylphosphonium $(Ph4P)^+$ salt of the pseudotetrahedral cobalt(II) complex $[Co(SPh)_4]^{2-}$.[20] The origin of slow relaxation of magnetization in $(Ph4P)_2[Co^{II}(SPh)_4]$ is based on its Kramers ground state along with the remarkably large axial ZFS shown by EPR and magnetic susceptibility measurements.[21−23] An even more anisotropic complex ($[Co(C_3S_5)_2]^{2-}$, $C_3S_5^{2-}$ = 4,5-dimercapto-1,3-dithiole-2-thione) with pseudotetrahedral $[Co^{II}S_4]$ core was recently reported to show SMM properties.[24] A first principal study on the origin of spin Hamiltonian (SH) parameters in the $[Co^{II}S_4]$ core containing complexes revealed strong magneto-structural correlations directly reflected in both the magnitude and sign of the ZFS upon structural variations involving the first and second coordination sphere.[25]

Besides the structural variation, the substitution of the donor atom can strongly affect the magnetic anisotropy. For example, the changes of the ligand donor atom (X) from oxygen to phosphorus or arsenic in $Co(XPh_3)_2I_2$ complexes dramatically alters the ZFS.[26]

A similar behavior was shown for the series $(Ph_4P)_2[Co^{II}(XPh)_4]$ (X = O, S, Se) where all compounds are reported to exhibit SMM properties.[27] Although the structures of the complexes are very similar, the magnetic and spectroscopic properties change significantly in the series X = O, S, Se.

Inspired from those studies, we report herein a systematic theoretical study of the magneto-structural correlations in $[Co^{II}(XPh)_4]^{2-}$ (X = O, S, Se, Te) based on multireference quantum chemical methods and ab initio based ligand field theory. The correlation of the ZFS with softness of the ligands, relativistic nephelauxetic effects, and covalency are discussed.

2. COMPUTATIONAL DETAILS

The ORCA[28,29] computational package was employed for all quantum chemical calculations. Geometry optimizations were performed using the pure BP86 functional,[30,31] with Ahlrichs polarized basis set def2-TZVP[32−34] and Grimme's dispersion correction D3.[35,36] The auxiliary basis set def2-TZVP/J was used in conjunction with the resolution of identity approximation.[37]

State-averaged complete active space self-consisted field (SA-CASSCF)[38−40] together with N-electron valence perturbation theory to second order (NEVPT2)[41−44] as well as the spectroscopy oriented configuration interaction (SORCI)[45] calculations were performed on top of the SA-CASSCF reference wave functions, in order to recover the major part of the differential dynamic correlation between the ground and the excited states. Scalar relativistic effects were taken into account by a standard second-order Douglas-Kroll-Hess[46] (DKH) procedure. The above protocols together with a segmented all-electron relativistically contracted version[47] of Ahlrichs polarized basis set def2-TZVP[32−34] were used for calculation of spin-free states. The minimal active space for the ab initio calculations should include the five 3d based molecular orbitals, involved in nonbonding or σ^* Co−S antibonding interactions. This leads to an active space of seven electrons in five orbitals CAS (7,5). We have included all 10 states for the $2S + 1 = 4$ (quartet) states arising from the ^4F and ^4P terms of Co(II), and all the 40 states for the respective $2S + 1 = 2$ (doublet) states arising from the ^2P, ^2D (twice), ^2F, ^2G, and ^2H terms of Co(II) ion. The resolution of identity approximation with corresponding correlation fitting of the basis set[37] was employed in order to speed up the calculations.

In order to determine the energies of the transitions, the Gaussian deconvolution of the experimental spectra was done with the orca_asa program (see the Supporting Information for details). In addition, to get the splitting of the *d*-orbitals, a ligand field analysis was performed via the recently developed ab initio ligand field theory used to analyze the splitting of *d*-orbitals.[17,48] To this end, the energy eigenvalues and eigenfunctions from CASSCF calculations were used to reconstruct the matrix of the ligand field Hamiltonian, which is parametrized in terms of the 5 × 5 one-electron ligand field matrix elements accounting for the splitting of the nominal 3*d*-orbitals due to interaction with the ligand donor atoms, as well as the Racah parameters B and C to take interelectronic repulsion into account. Since all matrix elements of the ligand field Hamiltonian matrix are linearly dependent on these parameters, the latter can be determined via a least-squares fitting method to the corresponding ab initio values of the same matrix elements.

The fine structure of the ground and the excited states was computed on the basis of the Breit-Pauli approximation where the spin−orbit coupling (SOC) Hamiltonian consists of one- and two-electron parts:

$$\hat{H}_{SO} = \frac{\alpha^2}{2}\sum_A\sum_i \frac{Z_A}{|\vec{R}_A - \vec{r}_i|^3}\hat{\vec{l}}_i^{\,A}\hat{\vec{s}}_i - \frac{\alpha^2}{2}\sum_i \hat{\vec{s}}_i \sum_{j\neq i}\frac{1}{|\vec{r}_i - \vec{r}_j|^3}(\hat{\vec{l}}_i^{\,j} + 2\hat{\vec{l}}_j^{\,i}) \tag{1}$$

where α is the fine structure constant, $\hat{\vec{l}}_i^{\,A} = (\vec{r}_i - \vec{R}_A) \times \vec{p}_i$ is the angular momentum of the *i*-th electron relative to nucleus *A* with charge Z_A at position $\vec{R}_A$, and $\hat{\vec{l}}_i^{\,j} = (\vec{r}_i - \vec{r}_j) \times \vec{p}_i$ is the angular momentum of the electron *i* relative to electron *j*.

In order to compute both, one- and two-electron contributions of the SOC operator, the mean field approximation (SOMF) was used,[49] where the SOC operator was effectively represented as the one-electron operator $\hat{H}_{SOMF} = \sum_i \hat{z}_i \hat{\vec{s}}_i$.

Alternatively, a less sophisticated treatment of SOC can be applied under the assumption that the two-electron term provides just a "screening" of the nuclear charge. Then, the overall SOC can be reduced to the one-electron operator

$$\hat{H}_{SO} = \sum_A\sum_i \xi(r_{iA})\hat{\vec{l}}_i^{\,A}\hat{\vec{s}}_i \tag{2}$$

where $\xi(r_{iA}) = (\alpha^2/2)(Z_{A\,eff}{}^2/(|\vec{r}_i - \vec{R}_A|^3))$ is an effective function of the spin−orbit coupling of electron *i* relative to the nucleus *A*. The parameters $Z_{A\,eff}$ are determined empirically. This approach allowed us to estimate the effect of heavy ligand atoms on the total ZFS by adjusting the corresponding effective nuclear charges.

The effective Hamiltonian approach[50,51] was used to compute SH parameters. On the one hand, the spitting of a spin multiplet without applied field can be described by the SH $\hat{H}_S = \hat{\vec{S}}\,\mathbf{D}\,\hat{\vec{S}}$, that acts in the Hilbert space $|S, M_S\rangle$ (**D** is the ZFS tensor). On the other hand, the energies of the "exact" spin−orbit states that correspond to the ground state spin multiplet can be projected to the model space $|\tilde{\Psi}_k\rangle$ with defined *S* and M_S values by effective Hamiltonian $\hat{H}_{eff}|\tilde{\Psi}_k\rangle = E_k|\tilde{\Psi}_k\rangle$. Therefore, by building one to one correspondence of the SH matrix elements with the effective Hamiltonian matrix elements from ab inito calculation, all 9 values of the ZFS tensor **D** can be directly extracted. However, this approach is only valid when the ground state is well isolated from the first excited state, implying that energy separation should be larger than the effective spin−orbit coupling constant.

Magnetic susceptibilities have been derived by following the procedure detailed in ref 52. In the basis of CASSCF/NEVPT2 computed 10 quartet and 40 doublet states, the matrix elements of SOC and Zeeman operators have been computed as

$$\langle\Psi_I^{SM_S}|\hat{H}_{BO} + \hat{H}_{SOC} + \hat{H}_Z|\Psi_J^{S'M_S'}\rangle = \delta_{IJ}\delta_{SS'}\delta_{M_SM_S'}E_I^S + \langle\Psi_I^{SM_S}|\hat{H}_{SOC} + \beta\vec{B}(\hat{\vec{L}} + g_e\hat{\vec{S}})|\Psi_J^{S'M_S'}\rangle \tag{3}$$

Diagonalization of this matrix leads to magnetic sublevels with generally mixed quantum numbers generated by the ladder operators for *x*- and *y*-components of *S* in the expressions for SOC and Zeeman

DOI: 10.1021/acs.inorgchem.5b01706
Inorg. Chem. 2015, 54, 9948−9961

Table 1. Selected Structural Parameters of the $[Co(XPh)_4](Ph_4P)_2$ Complexes

	ligand						
	O		S		Se		Te
geometry	X-ray	D_{2d}	X-ray	D_{2d}	X-ray	D_{2d}	D_{2d} (opt)
Co−X bond, Å	1.957	1.963	2.319	2.323	2.437	2.432	2.488
	1.966		2.329		2.425		
	1.970		2.313		2.429		
	1.957		2.331		2.437		
Co−X−C angle, deg	129.2	128.5	113.9	110.3	110.4	107.8	103.2
	124.8		108.6		107.6		
	126.2		109.8		106.6		
	133.6		108.8		106.5		
X−Co−X angle, deg	104.4	117.6[a]	119.6	115.6	121.0	116.6	118.3
	104.1		112.5		113.6		
	105.9		116.3		116.9		
	111.5		114.0		115.0		
	122.9	94.3[a]	97.4	97.8	94.3	96.0	92.9
	106.8		98.3		97.7		
X−Co−X−C torsion angle, deg	59.3	180.0	−152.1	180.0	−152.7	180.0	180.0
	−53.7		−170.6		−172.3		
	61.04		−169.8		−166.9		
	−132.0		−175.7		−178.4		

[a]The X−Co−X angles were adopted from the X-ray structure of $(PPh_4)K[Co(OPh)_4]$.[27]

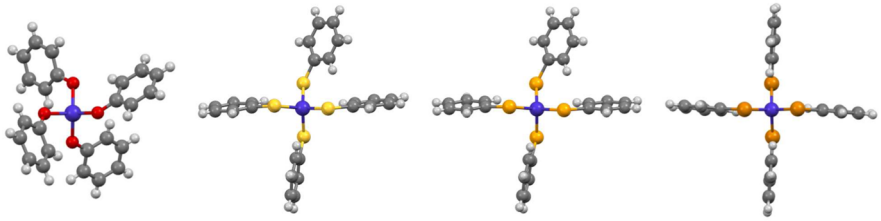

Figure 1. Molecular structures of Co^{II} complexes taken from X-ray diffraction for $(PPh_4)_2[Co(XPh)_4]$ with X = O, S, and Se and the DFT-optimized geometry of $[Co(TePh)_4]$ (Co, blue; O, red; S, yellow; Se, dark-yellow; Te, orange; C, dark-gray; H, gray).

interaction with the magnetic field. The magnetization of each state $i = \Psi_I^{SM_S}$ is computed as the first derivative of its energy with respect to the magnetic field along a fixed α direction $\mu_i^\alpha = \partial E_i/\partial B^\alpha$, and paramagnetic susceptibility for each state is computed as the second derivative $\chi_i^\alpha = \partial\mu_i^\alpha/\partial B^\alpha = (\partial^2 E_i/(\partial(B^\alpha)^2))$. Only the component along the applied field is estimated since only this component is measured in the experiment. All the derivatives are taken with the 5 step numerical differentiation procedure with the step size of 0.01 T at the experimental field (0.1 T). The average over all possible directions (α) of the magnetic field on the Lebedev grid with 434 points is comparable with the experimental powder measurements. The temperature dependence is coming from the ensemble averaging over all states according to the Boltzmann statistic

$$\chi(T) = \frac{\sum_i \chi_i e^{-E_i/kT}}{\sum_i e^{-E_i/kT}} \quad (4)$$

The explicit, direct treatment for all ground and excited states allows us to go beyond the SH approach, which would be valid only for energetically well-isolated ground state manifolds. By construction, this method includes also the temperature independent paramagnetism (TIP), which arises from mixing of nonpopulated excited magnetic states into the ground state levels caused by the magnetic field.

3. RESULTS AND ANALYSIS

3.1. Magnetic Properties of the Compounds. The compound $(Ph_4P)_2[Co(SPh)_4]$ was first synthesized and characterized by Holah and Coucouvanis,[53] later its magnetic properties were extensively studied by Fukui et al.[21−23] A first analysis of the temperature dependence of the molar powder magnetic susceptibility based on the SH

$$\hat{H} = D\left[\hat{S}_z^2 + \frac{E}{D}(\hat{S}_x^2 - \hat{S}_y^2)\right] + g_{\parallel}\beta H_z\hat{S}_z + g_{\perp}\beta H_{\perp}(\hat{S}_x + \hat{S}_y) \quad (5)$$

yielded very large axial ZFS ($D = -100(30)$ cm^{-1}, $E/D = 0$) and high anisotropy of the g-tensor ($g_{\parallel} = 3.13$ and $g_{\perp} = 2.25$).[21] Later, single crystal susceptibility measurements gave more accurate values of $D = -70(10)$ cm^{-1}, $g_{\parallel} = 2.7(1)$, and $g_{\perp} = 2.2(1)$, and the EPR on the doped single crystal with 10% Co/Zn allowed one to estimate the rhombicity parameter $E/D < 0.09$.[22] Almost two decades later, Zadrozny et al. showed that this compound exhibits slow magnetic relaxation without a magnetic bias field. They reported $D = -74$ cm^{-1}, $E/D < 0.01$, and $g = 2.7(1)$, extracted from fitting of their low temperature (2−7 K) high-field (1−7 T) powder magnetization data.[20]

Recently, the synthesis and structures of $(Ph_4P)_2[Co(OPh/SePh)_4]$ compounds have been reported.[27] Both compounds show slow relaxation of magnetization; however, the one with oxygen requires a biasing field. The reported analysis of the powder magnetic susceptibility shows that zero-field splitting (ZFS) increases dramatically within the series from oxygen to the more covalent S and Se donor atoms ($D = -11$, -62, and

DOI: 10.1021/acs.inorgchem.5b01706
Inorg. Chem. 2015, 54, 9948−9961

−83 cm^{-1} for O, S, and Se, respectively). The same trend is found for the anisotropy of the g-tensor ($g_{\parallel}$ = 2.222, 2.960, and 2.953, with $g_{\perp}$ = 2.118, 2.285, and 2.165 for O, S, and Se, respectively).[27]

3.2. Molecular Structures in the Ground State. The most important structural details of the cobalt coordination in the series $(Ph_4P)_2$ $[Co(XPh)_4]$ (X = O, S, Se)[16,53] are summarized in Table 1. For the sake of completeness, the hypothetical compound $[Co^{II}(TePh)_4]^{2-}$ is also included in the table, together with the corresponding parameters obtained from DFT optimization for the D_{2d} symmetrized complexes. The geometric structures of the $[Co(S/SePh)_4]^{2-}$ complexes appear to be rather similar, but the structure of $[Co(OPh)_4]^{2-}$ is more distorted than the others (Figure 1).

The most important structural variation in the series is the elongation of the metal−ligand bond due to increase of the covalent radii of the donor atom from oxygen to tellurium (the Co−X bonds for X = O, S, Se, and Te are 1.96, 2.32, 2.43, and 2.49 Å, respectively). The decrease of the angle Co−X−C in the series from 130° (X = O) up to 103° (X = Se) is mainly caused by the difference in hybridization of the chalcogen atomic orbitals, which will be discussed in more detail below.

The analysis of the available experimental data shows that the substitution of the oxygen donor by sulfur or selenium dramatically changes the magnetic and spectroscopic properties of the compounds. In order to separate the influence of symmetry effects on the term splitting from the effects of the different bonding interactions with the O, S, and Se ligating atoms, we have also analyzed the entire series of complexes by assuming ideal D_{2d} symmetry.

There are two important angles that characterize the molecular structures of the $Co(XC^R)_4$ cores, namely, the polar angle θ and the torsion angle ψ for each of the ligands (Figure 2). The polar angle θ is defined as the angle between

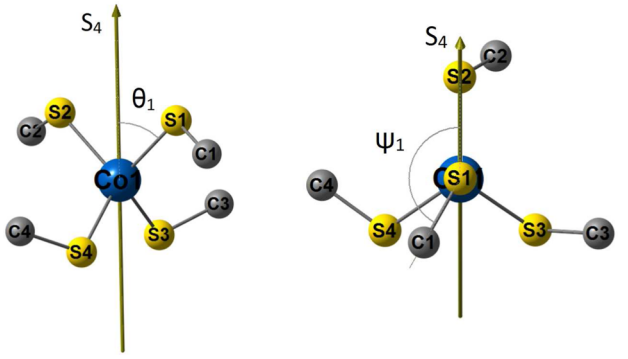

Figure 2. Schematic representation of the first and the second coordination sphere of Co ion (S_4 symmetry). The two angles θ_1 and ψ_1 define the position of ligand 1.

the S_4-rotation axis and the Co−X bond, for which the structures of $[Co(XPh)_4]$ complexes show $\theta_1 = \theta_2 = \theta$ and $\theta_3 = \theta_4 = 180 - \theta$, whereas in the symmetrized complexes θ is 47.5°.

The corresponding torsion angle ψ describes the angle between two planes: the first plane contains the S_4-rotation axis and the ligand atom X = O/S/Se, while the second plane is formed by Co, the atom X = O/S/Se, and the carbon atom bound to X ($\psi_1 = \psi_2 = 180 - \psi$ and $\psi_3 = \psi_4 = \psi$; in D_{2d} symmetry $\psi = 0$). Note that in the literature the positions of the carbon atoms are alternatively defined by the torsion angle ω between the X−Co−X−C planes.[25]

3.3. Electronic Structures of the Ground States. In order to rationalize the differences in electronic structures of the $[Co(XPh)_4]^{2-}$ dianions caused by the different ligand donor atom X, ab initio ligand field analyses have been performed for the symmetrized structures described above. This allows us to generate ligand field splitting diagrams from multireference ab initio calculations as described in detail in refs 17 and 48.

In a first approximation under ideal tetrahedral coordination around the cobalt center, one would expect to find the set of t_2 orbitals (d_{xy}, d_{xz}, d_{yz}) energetically higher than the set of double degenerate e-orbitals (d_{x2-y2}, d_{z2}). However, the situation is different for the present complexes, as the symmetry distortions and, more importantly, the anisotropies of the metal−ligand bonds lead to deviations from that pattern, which strongly affects the magnetic properties of the systems. In fact, however, the general pattern of ligand field splitting (Figure 3) is similar

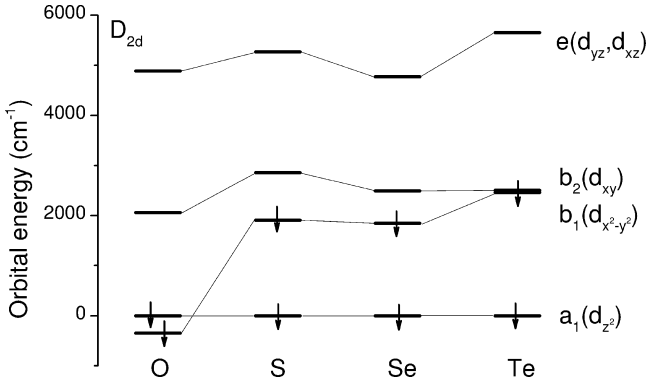

Figure 3. Energies of the d-orbitals of the D_{2d} symmetrized $[Co(XPh)_4]^{2-}$ complexes computed by ab initio LFT based on the CASSCF(7,5) solution for 10 quartet and 40 doublet states.

for all complexes. The orbitals with the highest energy are the degenerate d_{xz} and d_{yz} orbitals, being well separated from other 3d-orbitals. The key difference in the series with X = O, S, Se, and Te is the energetic separation of the d_{xy} and d_{x2-y2} orbitals. This splitting decreases dramatically from oxygen to tellurium. As expected, this orbital splitting is reflected in the energetic separation between ground and first excited states of the compounds. The ground state electron configurations are shown in Figure 3 with two β-electrons only; the five α-electrons that form half-filled d-shells are omitted for clarity. The resulting true symmetry of the ground states in the D_{2d} point group is $^4B_1$ throughout.

Conventionally, the strength of the ligand field can be measured by the 10Dq parameter, which is defined here as the separation between the barycenter of d_{z2}, d_{x2-y2} orbitals (e orbitals in T_d symmetry) and d_{xz}, d_{yz}, d_{xy} orbitals (t_2 orbitals in T_d), whereby 10Dq is taken as negative, which is usual for tetrahedral complexes.[54] The 10Dq parameter decreases along the series (Table 2), which is consistent with the fact that tellurium is known as a much softer ligand than oxygen.

Apparently, the d-orbital splitting depends not only on the type of the ligands but also on their positions. According to the angular overlap model (AOM; see Supporting Information for derivation and a comment), the ligand field energies in D_{2d} symmetry can be written as

DOI: 10.1021/acs.inorgchem.5b01706
Inorg. Chem. 2015, 54, 9948−9961

Table 2. AOM Parameters (cm^{-1}) for the D_{2d} Symmetrized $[Co(XPh)_4]^{2-}$ Complexes at the CASSCF(7,5) Level

X	B (cm^{-1})	C/B	Dq (cm^{-1})	e_σ	$e_{\pi s}$	$e_{\pi c}$	$e_{\pi\sigma c}$
O	1180	3.72	−412	4265	894	574	0
S	1148	3.71	−351	3164 (2624)	1026 (427)	41 (−449)	360 (0)
Se	1150	3.70	−309	2832 (2420)	983 (534)	26 (−341)	271 (0)
Te	1117	3.70	−284	3275 (3234)	1327 (1282)	0 (−37)	0 (0)

$$E(d_{z^2}) = \mathbf{e_\sigma(3\cos^2\theta - 1)^2 + 3e_{\pi c}\sin^2 2\theta} + [-\sqrt{3}\, e_{\pi\sigma c}\sin 2\theta(3\cos^2\theta - 1)] \quad (6)$$

$$E(d_{x^2-y^2}) = \mathbf{4e_{\pi s}\sin^2\theta}$$

$$E(d_{xy}) = \mathbf{3e_\sigma\sin^4\theta + e_{\pi c}\sin^2 2\theta} + [\sqrt{3}\, e_{\pi\sigma c}\sin 2\theta\sin^2\theta]$$

$$E(d_{xz}, d_{yz}) = \mathbf{\frac{3}{2}e_\sigma\sin^2 2\theta + 2e_{\pi s}\cos^2\theta + 2e_{\pi c}\cos^2 2\theta} + \left[\frac{\sqrt{3}}{2}e_{\pi\sigma c}\sin 4\theta\right]$$

At the most elementary level, the simple AOM model accounts for σ- and π-interaction of antibonding molecular orbitals in terms of three parameters: e_σ, $e_{\pi s}$ (π−Co−X−C out-of-plane bonding interaction), and $e_{\pi c}$ (π−Co−X−C in-plane bonding interaction), respectively (Figure 4). The terms

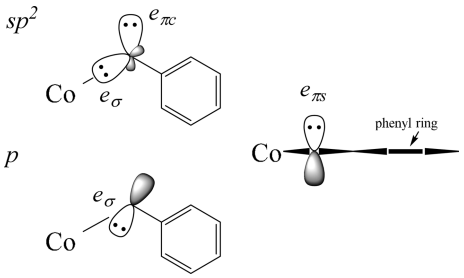

Figure 4. Ligand orbitals relevant for metal−ligand σ- and π-interaction for sp^2 hybridized and nonhybridized ligand orbitals.

belonging to this minimal model are marked bold in eq 6. However, this parametrization is only valid if the pseudosymmetry around a given metal−ligand bond is not lower than C_{2v}, which strictly would be the case only for monatomic ligand such as oxide (O^{2-}) and sulfide (S^{2-}).

It was shown for the SPh ligand[22] that the so-called misdirected valence should be taken into account. When for the sake of simplicity this is neglected, the AOM model leads to unphysical $e_{\pi c}$ parameters in our series with X = S, Se, and Te (Table 2 in brackets).

The more elaborate parametrization considers misalignment of metal and ligand orbitals in terms of additional parameters, which is encountered for all M−L arrangements with lower than C_{2v} − C_s or C_1 symmetry.[55] The basic concept was put forward and implemented into the formalism of ligand field theory by Liehr,[56] followed by applications to the interpretation of d−d spectra.[57,58] Accordingly, in the present study, where additional σ- and π-interactions with ligand orbitals in the Co−X−C plane (the C_s-symmetry plane) have to be considered, the additional, positively defined parameter $e_{\pi\sigma c}$ was introduced to this end (eq 6, terms are printed nonbold). The misdirected valence becomes important when the p-orbitals are not hybridized or weakly hybridized like in the case of S, Se, and Te in contrast to the sp^2-hybridized oxygen. Therefore, the $e_{\pi\sigma c}$ parameter is set to zero for oxygen while it was optimized for the other ligand atoms. In order to reduce the number of independent parameters in the latter case, the relation $e_{\pi\sigma c}^2 = e_{\pi c}e_\sigma$ was used. The values obtained from this analysis are listed in Table 2.

In accordance with the expectations for the sp^2 hybridized orbitals of oxygen, the values for $e_{\pi s}$ and $e_{\pi c}$ are comparable, while the $e_{\pi c}$ parameter goes to zero when the p-orbitals in the Co−X−C plane becomes nonhybridized, for the S, Se, and Te derivatives. The misdirected valence energy $e_{\pi\sigma c}$ decreases with decreasing Co−X−C angle (110°, 108°, and 103° for S, Se, and Te). For the S, Se, and Te ligands, the in-plane π antibonding energies $e_{\pi c}$ are small, as expected, but they follow the trends in the Co−X−C angles (vide supra).

Ab initio ligand field theory allows one not only to analyze d-orbital splitting but also to estimate the Racah parameters B and C for the interelectronic repulsion, which determine the energies of the excited quartet and doublet terms that arise from the d^7 configuration of Co^{II}. The values obtained for B and C are collected along with the ligand field parameters in Table 2.

3.4. Experimental and Theoretical *d*−*d* Spectra. An isolated Co^{II} ion has the electron configuration [Ar]$3d^7$, which gives 10 quartet and 40 doublet states. The ground term, ^4F, is separated from the first excited term, ^4P, due to the interelectronic repulsion within the 3d-shell. In terms of Racah parameters, the separation is 15B. The first doublet state, ^2G, has the energy 4B + 3C. Using the commonly employed estimate $C \approx 4B$,[59] the ^2G term is only 1B higher than ^4P. Other doublet states are higher in energy.

In the presence of a tetrahedral ligand field, the ^4F term is further split into $^4A_2$, $^4T_2$, and $^4T_1$ while the ^4P term correlates with $^4T_1$. According to the selection rules in the T_d point group, electric dipole transitions from the $^4A_2$ ground state are allowed only to $^4T_1$ states. Further lowering of the ligand field symmetry to D_{2d} leads to splitting of the triply degenerate states: T_1 splits into E, A_2, and T_2 splits into E, B_2. The symmetry of the ground state in D_{2d} is $^4B_1$, as mentioned above. Thus, among the quartet states only transitions to $^4B_2$ are electrically dipole forbidden. Any further symmetry lowering that destroys the S_4 rotational axis leads to splitting of the doubly degenerate E states (Figure 5).

The experimental NIR-vis spectra of $(PPh_4)_2[Co(XPh)_4]$ (X = O, S, Se) recorded from solid powders in diffuse reflection at room temperature in the range of 4500−20000 cm^{-1} display two main bands corresponding to $^4T_1(^4P)$ and $^4T_1(_4F)$ transitions (Figure 6).[27] Low temperature polarized vis-NIR spectra recorded with a 1% Co/Zn doped single crystal of a $(Ph_4P)_2[Co/Zn(SPh)_4]$ mixture shows at least four sharp transitions in the region of 14 000−16 000 cm^{-1}.[22] However, at room temperature powder spectra, these lines are not well resolved (Figure 6).

The analysis of the SORCI computed spectra shows that in the case of the oxygen ligand excited states of the $^4T_2(^4F)$ term

DOI: 10.1021/acs.inorgchem.5b01706
Inorg. Chem. 2015, 54, 9948−9961

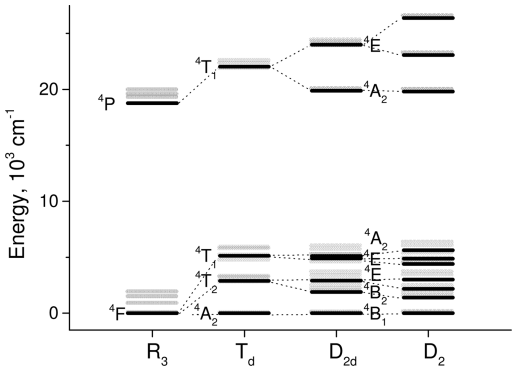

Figure 5. CASSCF(7,5) computed quartet terms of the Co^{II} ion (spherical symmetry, R_3) and terms for a hypothetical Co^{II} ion surrounded by four negative charges forming T_d symmetric, D_{2d} symmetric, and D_2 symmetric crystal fields. The result of additional SOC splitting is shown in gray.

are more isolated from the $^4T_1(^4F)$ term and transitions to the $^4T_2(^4F)$ states are less intense in the absorption spectrum compared to the other ligands. Therefore, all three individual transitions in the region of 5000−10 000 cm^{-1} obtained from a Gaussian deconvolution of the experimental band were assigned to the components of the $^4T_1(^4F)$ term. For S and Se, the $^4T_1(^4F)$ term strongly overlaps with the $^4T_2(^4F)$ term; therefore, the lowest observed transition was assigned to a part of the $^4T_2(^4F)$ term.

The components of the $^4T_1(^4P)$ term are also split into three due to symmetry lowering. In the case of $(PPh_4)_2[Co(OPh)_4]$, these three components are almost equidistant (~1000 cm^{-1}) that overemphasizes the effect of large distortion from D_{2d} symmetry, as also reflected by the X-ray structure. In the case of the SPh and SePh complexes, the pattern of the D_{2d} symmetry dominates.

In addition, Figure 6 demonstrates also the importance of SOC for gaining proper results. Indeed, SOC correction causes a blue shift of the calculated states and increased line broadening due to splitting of each quartet state into two doublets. Moreover, the spin-forbidden transitions gain intensity because SOC mixes doublet and quartet states. As a result, the corresponding doublet transitions overlap with the $^4T_1(^4P)$ band. Even though the intensities of the spin-forbidden transitions are small, they change the line shape of the $^4T_1(^4P)$ band because they are much sharper than the allowed transitions (Figure 6).

Furthermore, the energy positions of the parent $^4T_1(^4P)$ and $^4T_1(^4F)$ terms in an idealized tetrahedral symmetry, which can be assessed from the barycenters of the corresponding transitions, can be used to estimate the $10Dq$ and B parameters according to eqs 7 and 8:

$$E(^4T_1(F)) = 15Dq + \frac{15}{2}B - \frac{1}{2}\sqrt{225B^2 + 100Dq^2 - 180BDq} \quad (7)$$

$$E(^4T_1(P)) = 15Dq + \frac{15}{2}B + \frac{1}{2}\sqrt{225B^2 + 100Dq^2 - 180BDq} \quad (8)$$

In a previous analysis[27] of the spectra of $(PPh_4)_2$ [Co-$(SePh)_4$], the lowest band at 5500 cm^{-1} was assigned to the

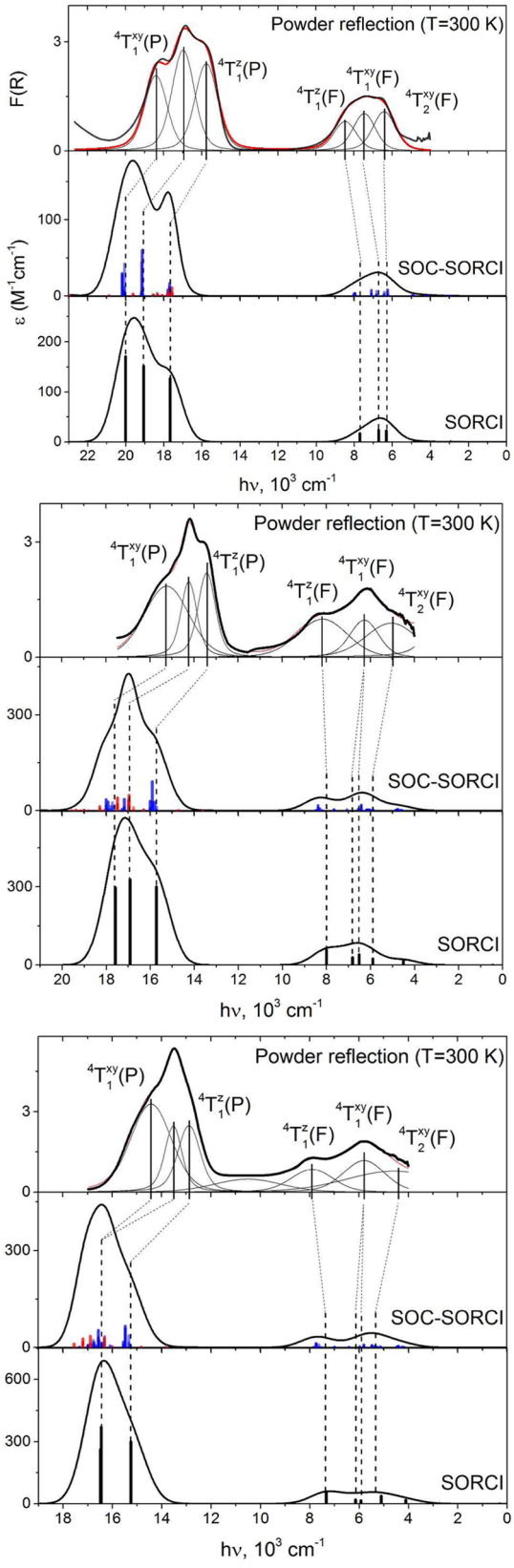

Figure 6. Gaussian deconvolution of the observed $d-d$ transitions in the NIR-vis spectra of $(PPh_4)_2[Co(XPh)_4]$,[27] with X = O (top panel), S (middle), Se (bottom). The computed SOC-SORCI spectra are in the middle of each panel (fwhm 1500 cm^{-1}); red sticks represent the spin-forbidden transitions (contribution of doublets >30%) with smaller line width (fwhm 900 cm^{-1}). The nonrelativistic SORCI computed spectra (fwhm 1500 cm^{-1}) are shown at the bottom.

DOI: 10.1021/acs.inorgchem.5b01706
Inorg. Chem. 2015, 54, 9948−9961

$^4T^{2x,y}$ component which has led to an overestimation of the 10*Dq* parameter and an underestimation of the Racah *B* parameter. There is a clear trend of reduction for the electron repulsion parameter *B* and the 10*Dq* in the series X = O, S, and Se. The decrease of 10*Dq* reflects a weakening of the ligand field through the series, while the reduction of *B* compared to the free ion value (B^0_{SORCI} = 1088 cm^{-1}) shows the increase of covalency (nephelauxetic effect). The SORCI-computed *B* parameters (Table 3) are much closer to the experiment than

Table 3. Energies (cm^{-1}) of the Excited States Experimentally Obtained from the Diffuse Reflectance Spectra Shown in Figure 6 and Theoretically Derived from SORCI Calculations, Shown Together with the Resulting *B* and 10 *Dq* Parameters[a]

	O		S		Se	
	exp.	calc.	exp.	calc.	exp.	calc.
$^4T_2(^4F)$		2932		461		307
		4180		4508		4115
		4872	~5000	5897	~4500	5106
$^4T_1(^4F)$	6326	6311	6201	6516	5667	5929
	7356	6717	6201	6820	5667	6147
	8376	7703	8008	8006	7806	7341
$^4T_1(^4P)$	15729	17679	13414	15720	12869	15252
	16948	19067	14228	16918	13513	16451
	18383	20006	15177	17591	14379	16489
Dq, cm^{-1}	−425	−396	−398	−411	−372	−373
B, cm^{-1}	773	930	610	768	586	757

[a]Derived from a best fit to the energies of $^4T_2$, $^4T_1(^4F)$, and $^4T_1(^4P)$ resulting from averaging of their sublevels split out by low symmetry.

those obtained from CASSCF (Table 2). The reduction of the interelectronic repulsion due to covalency of the metal−ligand bonds is underestimated by the CASSCF method because of too much ionic character of the wave function. Nevertheless, the 10*Dq* parameter and the energies of the $^4T_1(^4F)$ and $^4T_2(^4F)$ terms are in good agreement with the SORCI calculations and the trend in experimental values (Table S1).

The accurate prediction of the energy of the $^4T_1(^4P)$ states is a challenge because it is more sensitive to any lack of dynamical correlation than the lowest excited states. The SORCI method on the other hand has been proven successful in evaluating the visible and near-IR spectra of numerous transition metal complexes.[45,60,61] In order to decrease the computational cost, the SORCI calculations were performed for truncated model complexes where the phenyl groups are replaced by methyl groups and the positions of the atoms in the $[CoS_4C_4]$ core were left the same. However, the CASSCF energies of truncated and the full models are found to be essentially the same within ca. 100 cm^{-1} (Table S1).

3.5. Computed Magnetic Properties. On the basis of the X-ray structure of the $(Ph_4P)_2[Co(XPh)_4]$ (X = O, S, Se) compounds, we have computed the SH parameters of the Co(II) complexes using the scalar relativistic CASSCF/NEVPT2 methodology together with quasi-degenerate perturbation theory for the treatment of SOC and the effective operator technique for the analysis of the SH matrix as described under Computational Details (Table 4).

3.5.1. Magnetic Susceptibility. The energies of the lowest (nonrelativistic) excited states for all complexes are much larger than *kT* at room temperature (*NEVPT2*: 3632, 1541, and 1076 cm^{-1} for X = O, S, and Se, respectively), but even for X = Se, it

Table 4. SH Parameters of $[Co^{II}(XPh)_4]^{2-}$ (X = O, S, Se) Obtained from Temperature Dependence of Magnetic Susceptibility and EPR Data and Computed Values Obtained with CASSCF(7,5) and NEVPT2 Methods

		O	S	Se
D, cm^{-1}	expt.[22,27]	−11.1(3)	−62(1)/−70(10)	−83(1)
	CASSCF	−13	−59	−80
	NEVPT2	−12	−45	−66
E/*D*	expt.[22]	fixed at 0	fixed at 0/<0.09	fixed at 0
	CASSCF	0.15	0.03	0.01
	NEVPT2	0.13	0.03	0.02
g_x	expt.[22,27]	2.118(6)	2.285(4)/2.2(1)	2.165(5)
	CASSCF	2.242	2.183	2.149
	NEVPT2	2.199	2.130	2.112
g_y	CASSCF	2.292	2.237	2.195
	NEVPT2	2.236	2.172	2.148
g_z	expt.[22,27]	2.222(9)	2.960(3)/2.7(1)	2.953(3)
	CASSCF	2.421	2.902	3.112
	NEVPT2	2.350	2.692	2.901

is not an order of magnitude larger than the SOC constant for Co^{II} (530 cm^{-1}). Under these conditions, the SH formalism as defined in eq 5 is on the verge of being applicable.

In order to elucidate in detail the effect of the excited multiplets on the magnetic properties, we computed the temperature dependence of the magnetic susceptibility directly from the magnetic moments of all SOC-CASSCF/NEVPT2 magnetic states which are populated according to the Boltzmann statistics (eq 4.) This method can be applied even for orbitally degenerate ground states, where the standard SH formalism and perturbation theory fails.[62] We choose the system with the lowest energy of the first excited state, which is the $[Co(SePh)_4]^{2-}$ dianion. The result reproduces rather satisfactorily the experimental data of solid $(Ph_4P)_2[Co(SePh)_4]$ reported earlier (Figure 7, blue squares and black

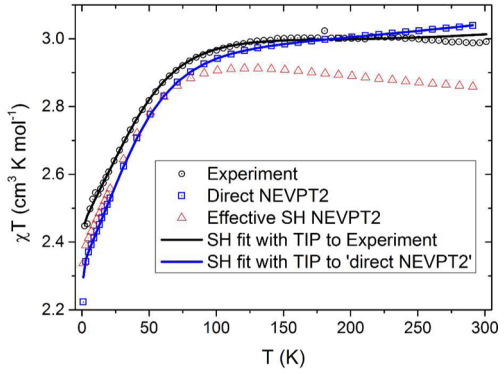

Figure 7. Temperature dependence of the molar magnetic susceptibility of the $(PPh_4)_2[Co(SePh)_4]$ (black circles).[27] The computed susceptibility based on all NEVPT2 states (blue squares) and the computed SH (*D* = −65.6 cm^{-1}, *E*/*D* = 0.015, and *g* = (2.1124, 2.1489, 2.9014)) from NEVPT2 calculation (red triangles).

circles).[27] In particular, the slope of the curve at low temperature and the temperature range where χT starts to level into a high-temperature plateau are well reproduced. These are the key features for the size of the ZFS.

Despite the agreement of the directly computed susceptibility curve with the experiment, the theoretical SH parameters obtained from the effective Hamiltonian analysis of the

DOI: 10.1021/acs.inorgchem.5b01706
Inorg. Chem. 2015, 54, 9948−9961

NEVPT2 states are quite different from the experimental values obtained previously (Table 4, column "Se"). Also, a magnetic susceptibility curve simulated with these theoretical SH parameters (Figure 7, red symbols) deviates significantly from the experiment (black circles), but interestingly, the deviation is even more from the result of the direct calculation (blue symbols). Superficially, this may not be unexpected in view of the low-lying first excited state, but the theoretical parameters (D = −65.6 cm^{-1} and E/D values = 0.015) nicely reproduce the calculated zero-field splitting of the ground state levels (Δ = 131.2 cm^{-1}, in which the SH formalism for S = 3/2 is equal to $2(D^2 + 2E^2)^{1/2}$). The difference of red and blue susceptibility curves (symbols) is the largest at high temperatures and appears to drop linearly with temperature. The effect must be due to a direct influence of the nonpopulated excited states on the ground state via the magnetic field, which is not covered by the SH given in eq 5. Since it is linear in χT vs T (cf. Figure 7, blue and red symbols), the corresponding contribution to χ is temperature-independent and is called TIP, temperature-independent paramagnetism. Since TIP is also found to be field-independent[63] (not shown here) it can be expressed as a uniform energy shift of all M_S sublevels which is quadratic in field. This contribution is also called Van Vleck susceptibility tensor $\chi_{\mu,\nu}{}^{VV}$, and up to second order perturbation theory, it can be expressed as the powder average of the tensor[63]

$$\chi_{\mu\nu}^{VV} = \frac{N}{V} 2\mu_B{}^2 \sum_J \frac{\langle 0|\hat{L}_\mu|J\rangle\langle J|\hat{L}_\nu|0\rangle}{E_J - E_0} \tag{9}$$

Here, μ_B is the Bohr magneton, $|0\rangle$ and $|J\rangle$ stand for the spatial part of the ground and excited state wave function (only states of the same multiplicity would contribute), and $\hat{L}_\mu$ is the μ-component of the orbital momentum operator; finally, E_J and E_0 are the energies of the excited and the ground states.

Conventionally, experimental magnetic susceptibility measurements are corrected for diamagnetic contributions to χ (negative in sign) and for temperature independent paramagnetism (TIP, positive in sign). The diamagnetic correction is typically estimated by using tabulated empirical Pascal's constants[64] for atoms and chemical groups of the sample, whereas TIP is normally not defined a priori but can be numerically fitted by using the high-temperature slope of χT. Reliable experimental TIP values are known only for closed-shell systems; for example, TIP measured for octahedral $[Co(III)(NH_3)_6]^{3+}$ is 200 × 10^{-6} cm^3 mol^{-1}.[65] In the previous study of $(PPh_4)_2[Co(XPh)_4]$, TIP was neglected (Figure 7, black circles).[27]

The significant deviation of the theoretical susceptibility data obtained directly and from theoretical SH parameters (Figure 7, blue and red symbols) suggests that TIP is large for $(PPh_4)_2[Co(SePh)_4]$ and should not be neglected. In order to obtain a theoretical estimate of TIP and furthermore to judge the putative influence of TIP on the reliability of SH simulations, we first performed a SH fitting of the directly obtained theoretical susceptibility curve (blue squares) by optimization all SH parameters as well as a TIP contribution to χ. The result (Figure 7, blue line) is a perfect fit with almost the same SH parameters as those deduced from the effective Hamiltonian analysis (D = −66 cm^{-1}, $g_\parallel$ = 2.875, and $g_\perp$ = 2.133), and the theoretical TIP value was found to be χ(TIP) = 708 × 10^{-6} cm^3 mol^{-1}. Moreover, corresponding refitting of the experimental data with TIP included (Figure 7, black line) yielded χ(TIP)exp = 616 × 10^{-6} cm^3 mol^{-1}, which is satisfactorily close to the theoretical value. As for the previous analysis, E/D was set to zero in this procedure and the g values were constrained to $g_x = g_y$. The reoptimized experimental ZFS parameter was found to be lower than previously, D = −74 cm^{-1}, instead of −83 cm^{-1} without TIP; $g_\parallel$ = 2.95 is similar to the previous results, but the anisotropy of the tensor $g_\parallel/g_\perp$ = 1.44 is larger than the ratio of 1.36 found without TIP. In summary, the theoretical approach described above allows one to evaluate the TIP effect (Van Vleck susceptibility) and to substantiate the SH model for the analysis of the experimental data.

3.5.2. Zero-Field Splitting. The computed SH parameters are in reasonably good agreement with the experiment in spite of the discussed limitations of the SH formalism. In this comparison, the CASSCF method gives systematically higher values for $|D|$ and g than the NEVPT2 approach (Table 4).

The ab initio methods allow us not only to reproduce the magnetic properties measured in the experiments but also to analyze in detail different contributions to the total ZFS. Preliminary calculations show that the spin−spin coupling contribution to D is <1 cm^{-1}, which means that ZFS arises essentially only from SOC. A closer analysis of the contributions to D from different excited states reveals that for the considered compounds the ZFS of the ground state is dominated by coupling with the three lowest excited states ($^4T_2$) (Table 5).

Table 5. Absolute Largest Contributions to D (cm^{-1}) from the Excited States of $[Co^{II}(XPh)_4]^{2-}$ (X = O, S, Se) Computed for the X-ray Structures by CASSCF/NEVPT2

	O	S	Se
$^4T_2$(F)	−36	−66	−88
	11	9	9
	11	6	6
$^2T_2$(G)	4	7	6
	−2	−2	−2
	−2	−2	−2

These contributions in fact capture 95% of D in the case of the OPh ligand, implying that the contribution from doublet states is negative. In the case of SPh and SePh ligands, the contribution from $^4T_2$ states is 105% of D. The overshooting is compensated by the positive contributions to D arising from the other quartet and doublet states.

The observation is not surprising and can be understood by considering simple group theoretical arguments. Due to the pseudotetrahedral local symmetry around the cobalt center, the angular momentum operator is a pseudovector and transforms under the irreducible representation T_1 in tetrahedral symmetry. Therefore, only T_2 terms can be mixed with the $^4A_2$ ground state via SOC. It should be stressed however that the ZFS of the ground $^4A_2$ state is exactly zero in ideal T_d symmetry. This is because the negative contribution to ZFS arising from the z-component of orbital momentum is completely canceled by the positive contributions arising from x- and y-components, respectively.

On the other hand, slight distortions of the D_{2d} symmetry split the T_2 term into B_2 and E terms. The $^4B_2$ states mix with the ground state (now $^4B_1$) via the z-component of the orbital momentum and give a negative contribution to D, likewise the mixing with ^4E gives a positive contribution to D. Depending on the energy order of $^4B_2$ and ^4E states (from $^4T_2$), the total D

DOI: 10.1021/acs.inorgchem.5b01706
Inorg. Chem. 2015, 54, 9948−9961

can be either negative or positive. Any further distortion that lifts the E state degeneracy leads to nonzero E/D values.

In an effort to further analyze the effects of the geometry distortion and the substitution of the ligand donor atom on the ZFS, we also computed SH parameters of the D_{2d} symmetrized structures as discussed in Section 3.2. As shown on Figure 8,

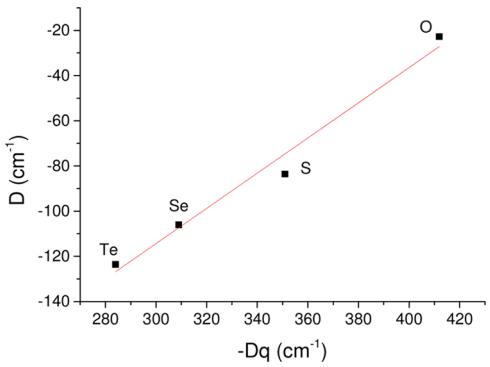

Figure 8. Correlation of the ZFS (D) and the strength of the ligand field (Dq) computed for D_{2d} symmetric structures obtained with CASSCF(7,5). The linear fit has an intercept with the y-axis at D ($10Dq$ = 0)= −350(30) cm^{-1} and a slope of 0.8(1).

there is a clear correlation of the ZFS and the $10Dq$ parameter extracted from the ab initio ligand field analysis (Table 2). Of course, also the intrinsic anisotropies of the coordinated ligand atoms play an essential role for ZFS. This effect will be discussed in more detail below.

The ZFS of the symmetrized structures is significantly larger than for nonsymmetric structures of the real complexes (Figure 9, black and red). However, before we move to the discussion

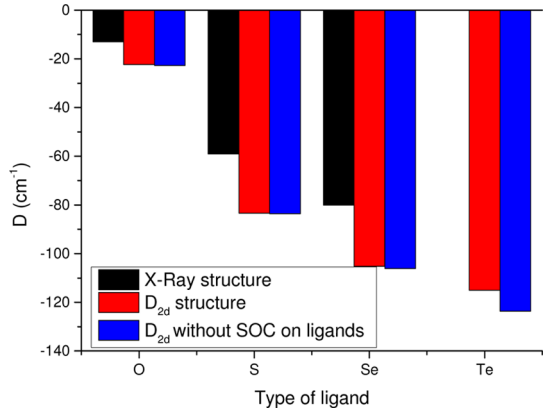

Figure 9. D values of the ZFS computed without SOC on the ligands. The X-ray structures, symmetrized to D_{2d} symmetry, have been used with CASSCF(7,5).

of the magneto-structural correlations, it is interesting to elucidate the importance of SOC at the ligand atoms to total D.

Surprisingly, switching-off the intrinsic spin−orbit coupling on the ligands (Figure 9) leads to an increase of the absolute value of D. However, the effect is small, amounting to ∼8% in the case of Te, while for the O, S, and Se it is rather negligible.

3.6. Qualitative Magneto-Structural Correlations. As emphasized in the previous section, the axial ZFS in the quasi-tetrahedral Co^{II} complexes described by the parameter D is largely governed by the splitting of the $^4T_2$ excited state due to axial D_{2d}/S_4 symmetry distortions, which then mix into the $^4A_2$ ground state via spin−orbit coupling. Perturbation theory shows that the sign of D depends on the energies of the two terms $E(^4T_2,z)$ and $E(^4T_2,x,y)$ (eq 10), which stabilize either the M_s = ±3/2 or the M_s = ±1/2 ground state magnetic sublevels, respectively. Negative values of $E(^4T_2z) - E(^4T_2x, y)$ ($^4T_{2,z}$ lower in energy than $^4T_{2,x,y}$) are associated with a negative D value and vice versa. The dependence of the state energies $E(^4T_2z) - E(^4T_2x, y)$ on the orbital energies as given by eq 11 shows that negative D values correlate with the order $d_{xz,yz} > d_{xy}$ and $d_{x2-y2} > d_{z2}$. There is chemical information involved because the orbital energy differences $e(d_{xy}) - e(d_{xz,yz})$ and $e(d_{z2}) - e(d_{x2-y2})$ depend both on metal−ligand π-antibonding and on the geometry. Focusing first on the effect of the symmetry on D, Figures 10 and 11 depict the orbital

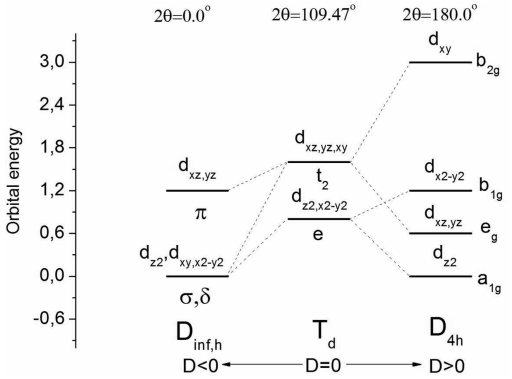

Figure 10. Correlation diagram for 3d-orbital energies in perfect T_d geometry and T_d with tetragonal elongation (left, linear arrangement) and tetragonal compression (right, square planar geometry); the diagram has been constructed by adapting isotropic metal−ligand π-interactions ($e_{\pi s} = e_{\pi c} = e_\pi$) and an e_π/e_σ ratio of 0.3; orbital energies are given in units of e_σ.

energies in dependence of the geometric distortions quantified by the angles 2θ and ψ. Tetragonal elongations/compressions described by angles 2θ larger/smaller than the tetrahedral value $2\theta_{Td}$ = 109.47° induce negative/positive D values. Thus, the negative sign of D found in all considered complexes correlates with the rather acute angle $2\theta \approx 95°$. Note that in contrast to

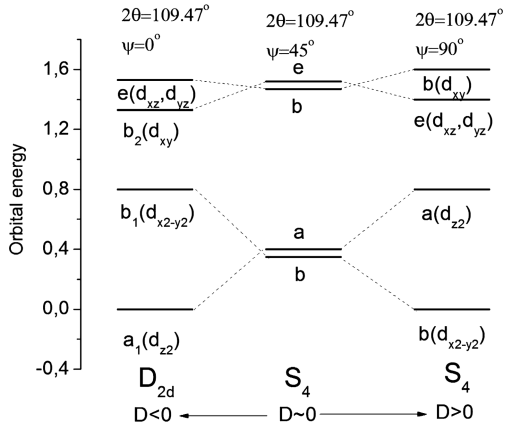

Figure 11. 3d-orbital energy diagram for a model complex with fully π-anisotropic metal−ligand bonds ($e_{\pi s} > 0$, $e_{\pi c} = 0$) relating the limiting D_{2d} geometries ($\psi = 0°$ left, $\psi = 180°$ right) with pseudotetrahedral S_4 geometry ($\psi = 45°$, pseudoisotropic π-ligators). The diagram has been constructed with $e_{\pi s}/e_\sigma$ = 0.3; orbital energies are given in units of e_σ.

DOI: 10.1021/acs.inorgchem.5b01706
Inorg. Chem. 2015, 54, 9948−9961

the situation for $[Co(OPh)_4]^{2-}$ with nearly isotropic Co−O π-interactions, both differences, $e(d_{xy}) - e(d_{xz,yz})$ and $e(d_{z2}) - e(d_{x2-y2})$, are negative for the series $[Co(XPh)_4]^{2-}$ (X = S, Se, Te) (see Figure 5). Their effects add to the increasing negative D value, whereas for the OPh derivative $e(d_{z2}) - e(d_{x2-y2})$ is small and positive and thus compensates the effect of the negative $e(d_{xy}) - e(d_{xz,yz})$ term. In summary, this leads to relatively low values of D for the $[Co(OPh)_4]^{2-}$ dianion.

Figure 11 shows the effect of the ligand twist angle ψ on the sign of D. This can be seen best for the complexes with pronounced π anisotropy of the Co−X bond, X = S, Se, and Te ($e_{\pi s}$ > 900 cm^{-1}, $e_{\pi c}$ close to zero). For the sake of simplicity, only idealized ligand positions corresponding to T_d geometry (2θ = 109.47°) have been taken into account. A simple expression for D in terms of ψ and of the Co−X−C out-of-plane energy $e_{\pi s}$, given by eq 12, nicely rationalizes the variation of D from negative values for ψ = 0° (close to the D_{2d} symmetrized geometries in the considered complexes) to positive values for ψ = 90°. Zero crossing occurs for ψ = 45°, which corresponds to pseudo isotropic π-antibonding. (A generalization of eq 12 is found in eqs S6−S15.) It is remarkable that for this type of magnetic anisotropy D does not vanish at the tetrahedral angle 2θ = 109.47° (ψ = 0°). In contrast, D is negative there and scales with the value of the $e_{\pi s}$ parameter (eq 12). In comparison to $[Co(OPh)_4]^{2-}$, which has almost isotropic π-bonding (D = 0, 2θ = 109.47°; see Figure 10), in other cases, significant distortions toward compressed D_{2d} geometries would be required to compensate for the πs-anisotropy such that D would become zero. We can conclude that for the S, Se, and Te donors, the πs-anisotropy extends the range of negative D values. This is strongly supported by quantitative calculations in the next section.

$$D(^4T_2) = \frac{4}{9}\zeta_{eff}{}^2\frac{E(^4T_2z) - E(^4T_2x, y)}{(10Dq)^2} \quad (10)$$

$$E(^4T_2z) - E(^4T_2x, y) = e(d_{xy}) - e(d_{xz,yz}) + (3/4)[e(d_{z2}) - e(d_{x2-y2})] \quad (11)$$

$$D(S_4) = -\frac{4}{9}\zeta_{eff}{}^2\frac{(8/3)e_{\pi s}\cos(2\psi)}{(10Dq)^2};$$
$$10Dq \approx (4/3)e_\sigma - (8/9)e_{\pi s}; \quad e_{\pi c} = 0;$$
$$2\theta = 109.47^0 \quad (12)$$

Completing this section, we note that in practice symmetry distortions as described by 2θ and ψ are mutually correlated because of steric repulsions between the bulky phenyl substituents which increase from the most favorable D_{2d} geometry with ψ = 0 to S_4-symmetry with ψ = 90°. For larger values of ψ, the resulting covariance of ψ and 2θ amplifies to the point where eventually the sign of D turns from negative to positive. This will be the subject of a quantitative analysis in the next section.

3.7. Effect of Bonding on the Magnetic Anisotropy. Magnetic anisotropies reflected by the reported and computed values of D in the complexes $Co(SPh)_4^{2-}$ and $Co(SePh)_4^{2-}$ are surprisingly large in view of the nondegenerate ground states. As follows from the qualitative discussion of the preceding section, this can be attributed to both, π-anisotropy of the Co−X bonds and elongated geometries with acute angles θ. Both effects lead to a stabilization of the $^4B_2(^4T_2)$ excited state with respect to the $^4B_1$ ($^4A_2$) ground states. When the energy gap $^4B_2$-$^4B_1$ becomes comparable with the effective spin−orbit coupling constant ζ_{eff}, the anisotropy increases strongly in the z-direction. Within the series of complexes, the gap decreases in the order of the donor atoms X = O to S to Se to Te, whereas D shows the opposite trend, as expected (Figure 12, top).

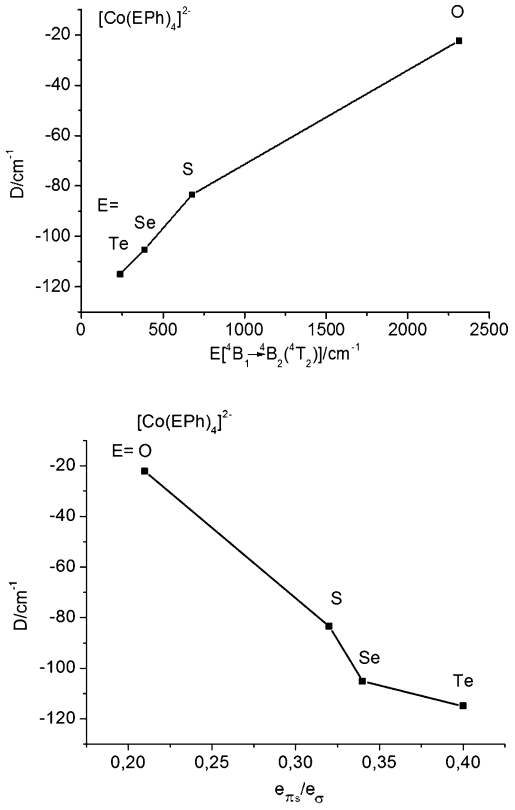

Figure 12. Correlation between D and the $[^4B_1(^4A_2) \rightarrow {}^4B_2(^4T_2)]$ energy gap (top) and between D and the ratio $e_{\pi s}/e_\sigma$ (bottom) for the four $[Co(XPh)_4]^{2-}$ complexes (X = O, S, Se, Te), obtained with CASSCF.

Moreover, when the angle 2θ is fixed to 95°, which is similar to the experimental situation in the four complexes, the trend in D correlates also with the relative importance of anisotropic π Co-ligand bonding (Figure 12, bottom); computed values of the $e_{\pi s}/e_\sigma$ ratio increase in the same order. The effective spin−orbit coupling energies ζ_{eff} are found significantly reduced in the complexes, compared with the spin−orbit coupling parameter ζ_o of the free Co^{2+} ion. This reduction increases with increasing metal−ligand covalence, again in the order X = O, S, Se, and Te (ζ_{eff} = −438, −433, −422, and −391 cm^{-1}, respectively, CASSCF results), which is known as the relativistic nephelauxetic effect.[11] However, the reduction does not supersede the trend in D arising from Co−X bonding (Figure 12, bottom). A comparison of the values D = −53.3 cm^{-1} and −67.1 cm^{-1}, computed for $[Co(SPh)_4]^{2-}$ and $[Co(SePh)_4]^{2-}$ with appreciable $e_{\sigma\pi c}$ (360 and 271 cm^{-1}, respectively), with the values D = −79.0 cm^{-1} and −91.5 cm^{-1} obtained from model calculations with $e_{\sigma\pi c}$ = 0 reveals that misdirected σ−π bonds are not in favor of magnetic anisotropy but reduce it. Apparently, the absence of such bonds in $[Co(TePh)_4]^{2-}$ ($e_{\sigma\pi c}$ is zero; see Table 2) correlates with the highest anisotropy of this complex in the series (Figure 12).

DOI: 10.1021/acs.inorgchem.5b01706
Inorg. Chem. 2015, 54, 9948−9961

3.8. Effect of Geometric Distortions on the Magnetic Anisotropy. The ligand field analysis together with AOM considerations shows that the key difference between the phenolate and thio(seleno)phenolate ligands is a lack of hybridization of the chalcogen atoms in the latter. Therefore, the effect of the structural variation is different for the two types of ligands.

The dependences of the total energy of the molecules in the ground state, of the relative energies of the split components of the $^4T_2$ excited state, and of D on the angle 2θ are depicted in Figure 13. In these computations, we have used a D_{2d} symmetrized structure, constraining the torsion angle to ψ = 0°. The variation of D with 2θ follows the π electron density, starting with the almost isotropic case encountered for the oxygen donor ligand. This is in support of the qualitative consideration in the proceeding section. At 2θ = 109.5°, the ^4E and $^4B_2$ terms ($^4T_2$) intersect, as expected for ideal tetrahedral geometry, and the ZFS parameter D vanishes. The total energy (E) in the ground state shows a shallow minimum with an optimized structure at 2θ angles of 100−105°.

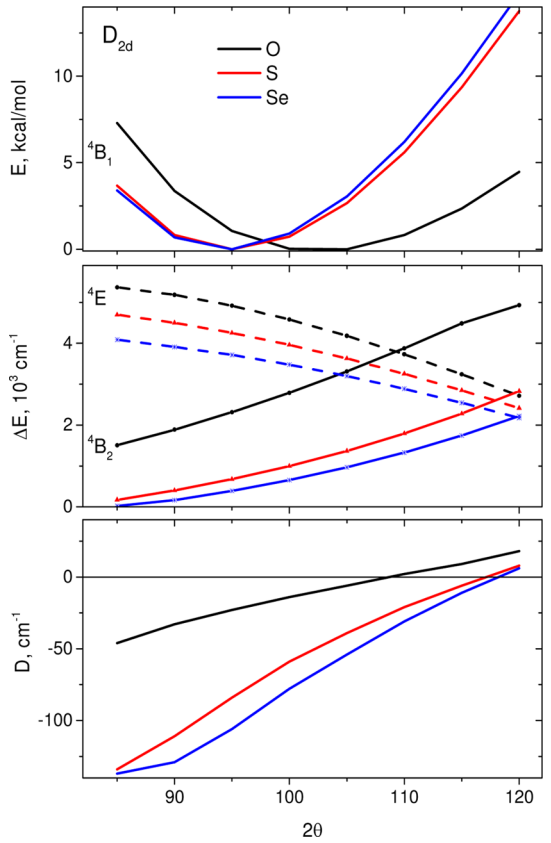

Figure 13. Variation of the 2θ angle in D_{2d} symmetrized structures. Top, the ground state energy; middle, the energies of the excited stated with respect to the ground state; bottom, the computed ZFS (CASSCF(7,5)).

Unlike the oxygen ligand, the S and Se atoms are not hybridized, which causes anisotropic π-interaction with the Co ion. Due to this π anisotropy, the parameter D is nonzero ($D \approx -50$ cm^{-1}) at tetrahedral geometry of the first coordination shell, again in agreement with the qualitative arguments from above (see Figure 11). The effects of the geometry and of the πs interaction on D cancel each other at $2\theta \sim 118°$, but the optimal structure corresponds to the $2\theta \sim 95°$, close to the experimentally observed values. The acute θ angles explain the large negative D values observed for the complexes.

In agreement with eq 12 of the proceeding section, the variation of the torsion angle ψ leads to dramatic changes in ZFS in the case of the Co−X bonds with high π anisotropy (X = S, Se; Figure 14). This is the reason why the same complex

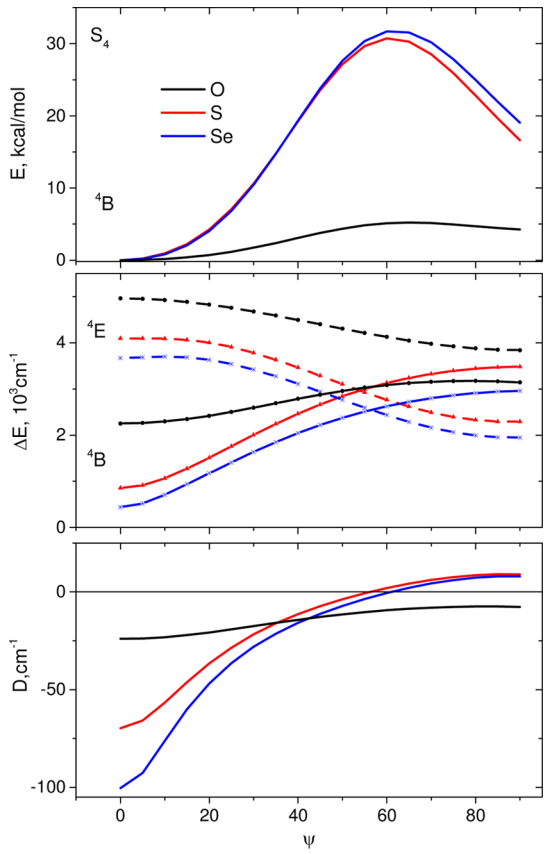

Figure 14. Variation of the torsion angle ψ in S_4 symmetrized structures (2θ = 94°, 98°, 96° for O, S, Se). Top, the ground state energy; middle, the energies of the excited stated with respect to the ground state; bottom, the computed ZFS (CASSCF(7,5)).

$[Co(SPh)_4]^{2-}$ with other *counter* ions such as $(Me_4N_2)^{2+}{}_2$ and $(Et_4N_2)^{2+}{}_2$ exhibits much smaller ZFS (D = 6.5 and 5.0 cm^{-1}).[66] In fact, the counterions affect the orientation of the nonrigid thiophenolate ligands. As shown by the angular overlap model[22,23] and high-level quantum chemical methods,[25] the ZFS of the $[Co^{II}SC^{R}]^{2-}$ core depends strongly on the S−Co−S polar angles and on the S−Co−S−C torsion angles. As a consequence, by assuming 4-fold symmetry for the CoS_4 core, the axial ZFS of the $[Co^{II}SC^{R}]$ core can be in a range from −100 up to +50 cm^{-1} (with E/D = 0), depending on the S−Co−S−C torsion angle. Lowering of the symmetry down to 2-fold or less enlarges the nonaxial contribution to the ZFS up to E/D = 0.33.[25]

From the potential energy surface, it is clear that the barrier for the rotation of the phenyl rings is about five times higher for the S and Se derivatives than for the oxygen based ligand (see nonrelaxed scan in Figure 14). This explains the more distorted molecular structure of $(PPh_4)_2[Co(OPh)_4]$. Corresponding correlations of the electronic structure with the torsion angle were found to play an essential role for the quasi-tetrahedral iron(II) complexes with cysteine−sulfur coordination in the archetypical iron−sulfur protein rubredoxin.[67] A DFT and

DOI: 10.1021/acs.inorgchem.5b01706
Inorg. Chem. 2015, 54, 9948−9961

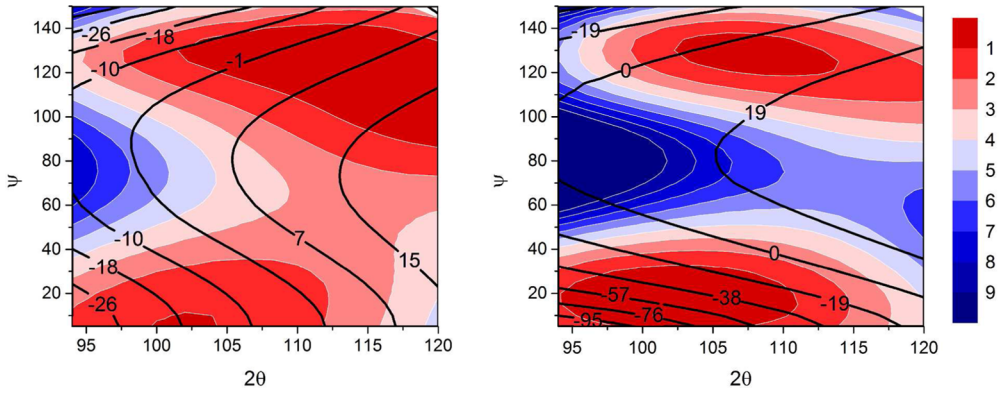

Figure 15. Two-dimensional relaxed potential energy surface scan (shown in colors according to color code on the right in kcal/mol) and the corresponding values of the zero-field splitting (black contour lines in cm^{-1}) of the $[Co(OMe)_4]^{2-}$ (left) and $[Co(SeMe)_4]^{-2}$ (right) model complexes.

AOM study of the corresponding synthetic model complex $[Fe(SCH_3)_4]^{2-}$ revealed the same two minima on the potential energy surface with respect to the torsion angles S−Fe−S−C.[68] The π anisotropy of the oxygen atom in $(PPh_4)_2[Co(OPh)_4]$ is small, which prevents crossing of the ^4E and ^4B terms ($^4T_2$) as a function of the ψ angle (Figure 14, middle panel), so that the D value remains moderate in the range between −25 and −5 cm^{-1}.

For the S and Se derivatives, a crossing of the ^4E and ^4B terms occurs at $\psi \sim 55°$ where D becomes zero, but this structure is unlikely to appear in real compounds since these geometries are far from minima on the potential energy surface. It is interesting to look at the full potential energy surface where both angles can vary simultaneously (Figure 15). For this purpose, we have carried out a two-dimensional relaxed scan along θ and ψ angles (see Section 3.2) followed by SA-CASSCF calculations for the truncated models $[Co(OMe)_4]^{2-}$ and $[Co(SeMe)_4]^{-2}$. The angles for all ligands were changed in a concerted way in order to preserve S_4 symmetry. There are two minima on the potential energy surface: one is close to the case of a compressed tetrahedron with large ligand torsion, $\psi \sim 130°$, and another is close to the case of an elongated tetrahedron without torsion, $\psi \sim 0°$ for $[Co(OMe)_4]^{2-}$ and $\psi \sim 20°$ for $[Co(SeMe)_4]^{-2}$.

In the case of the oxygen derivative, the local minima are very shallow, and the barrier between them is very low (<3 kcal/mol) so that the corresponding structures could be easily distorted. The structures close to the minimum for the elongated tetrahedron ($2\theta < 109.47°$) and small ψ angle are expected to exhibit negative D values, whereas the structures close to the second minimum (compressed tetrahedra) are likely to have the positive D.

The potential minima for the Se derivative are more local than those of the oxygen based compound, and the barrier is much higher. The D value drops down very fast for small ψ angles, once the tetrahedron becomes is elongated, and it can reach −100 cm^{-1}. The second minimum has larger θ angles, but the values are mostly still below the limit for nondistorted symmetry, i.e., $\theta = 109.47°$. Because of the large torsion angle $\psi \approx 130°$, D is positive for this minimum.

4. CONCLUSIONS

In this work, the origin of the magnetic anisotropy in four related complex dianions $[Co(XPh)4]^{2-}$ (X = O, S, Se, Te) with SMM behavior has been explored. Using correlated multireference ab initio calculations coupled to ab initio ligand field analyses, we were able to quantitatively reproduce and qualitatively analyze the experimentally determined axial ZFS parameter D measured for these compounds. Moreover, we have performed an extensive ligand field theory study on the four complexes involving determination of the ligand field parameters and the ab initio ligand field orbital energies followed by an angular overlap model analysis. In this way, we were able to subdivide the given ligands into two categories: the nearly isotropic π-donor ligand OPh^- and the mostly π-anisotropic SPh^- and $SePh^-$ ligands with ligand fields dominated by σ and Co−S/Se out-of-plane π-interactions. The negative ZFS parameter D increases across the series from O, S, Se and Te, in correlation with the relative increasing importance of π-bonding in this direction.

In particular, the angular overlap model parameters extracted from a best fit to CASSCF ab initio wave functions and energy eigenvalues allowed us to separate symmetry from bonding effects to zero-field splitting (ZFS). Tetragonally elongated/compressed D_{2d} geometries are shown to induce negative/positive D values in the case of the π-isotropic ligand in $[Co(OPh)_4]^{2-}$. For the Co^{II} complexes with the π-anisotropic ligands XPh^{1-}(X = S, Se, Te), *both*, geometry and π-anisotropy, are found to affect D. Anisotropic π-bonding extends the range of negative D values for distortions ranging from elongated to considerably compressed (up to $2\theta = 117°$) geometries. Moreover, rather large π-anisotropy is found to be responsible for the variation of D, dependent on the second coordination sphere of Co^{II} and quantified by the dihedral angle $\psi = \angle$ z−Co−X−C (X = S, Se, Te, the torsion angle); it maximizes negative D values for $\psi = 0°$, while it maximizes positive D values for $\psi = 90°$. Deviations from the axial geometry as observed in the reported X-ray structures lead to smaller negative D values and small, yet significant values of E/D.

Taken together, this work demonstrates the efficiency of the ab initio methods which when combined with proper ligand field analyses allows one to predict magnetic properties and to derive magneto-structural correlations. In a broader perspective, such a protocol can be applied to other series of transition metal complexes providing a quantitative tool with general applicability in the fields of (bio)inorganic and materials science chemistry.

DOI: 10.1021/acs.inorgchem.5b01706
Inorg. Chem. 2015, 54, 9948−9961

■ ASSOCIATED CONTENT

Supporting Information

The Supporting Information is available free of charge on the ACS Publications website at DOI: 10.1021/acs.inorgchem.5b01706.

Experimental and computed energies of the excited states; the input files and geometries; angular overlap model considerations (PDF)

■ AUTHOR INFORMATION

Corresponding Authors

*E-mail: frank.neese@cec.mpg.de.
*E-mail: mihail.atanasov@cec.mpg.de.

Notes

The authors declare no competing financial interest.

■ ACKNOWLEDGMENTS

This work is supported by Max Plank Society. Authors are grateful to J. Zadrozny and J. Long for providing spectroscopic and magnetic susceptibility data.

■ REFERENCES

(1) Layfield, R. A. *Organometallics* **2014**, *33*, 1084−1099.
(2) Coronado, E. *Molecular Magnetism: From Molecular Assemblies to the Devices*; Springer: Dordrecht, 1996.
(3) Gatteschi, D.; Sessoli, R.; Villain, J. *Molecular Nanomagnets*; Oxford University Press: Oxford, 2006.
(4) Bogani, L.; Wernsdorfer, W. *Nat. Mater.* **2008**, *7*, 179−186.
(5) Neese, F.; Pantazis, D. A. *Faraday Discuss.* **2011**, *148*, 229−238.
(6) Zadrozny, J. M.; Xiao, D. J.; Atanasov, M.; Long, G. J.; Grandjean, F.; Neese, F.; Long, J. R. *Nat. Chem.* **2013**, *5*, 577−581.
(7) Sessoli, R.; Gatteschi, D.; Caneschi, A.; Novak, M. A. *Nature* **1993**, *365*, 141−143.
(8) Murugesu, M.; Habrych, M.; Wernsdorfer, W.; Abboud, K. A.; Christou, G. *J. Am. Chem. Soc.* **2004**, *126*, 4766−4767.
(9) Tasiopoulos, A. J.; Vinslava, A.; Wernsdorfer, W.; Abboud, K. A.; Christou, G. *Angew. Chem.* **2004**, *116*, 2169−2173.
(10) Ako, A. M.; Hewitt, I. J.; Mereacre, V.; Clérac, R.; Wernsdorfer, W.; Anson, C. E.; Powell, A. K. *Angew. Chem., Int. Ed.* **2006**, *45*, 4926−4929.
(11) Neese, F.; Solomon, E. I. *Inorg. Chem.* **1998**, *37*, 6568−6582.
(12) Cirera, J.; Ruiz, E.; Alvarez, S.; Neese, F.; Kortus, J. *Chem. - Eur. J.* **2009**, *15*, 4078−4087.
(13) Waldmann, O. *Inorg. Chem.* **2007**, *46*, 10035−10037.
(14) Ishikawa, N.; Sugita, M.; Ishikawa, T.; Koshihara, S.-y.; Kaizu, Y. *J. Am. Chem. Soc.* **2003**, *125*, 8694−8695.
(15) Harman, W. H.; Harris, T. D.; Freedman, D. E.; Fong, H.; Chang, A.; Rinehart, J. D.; Ozarowski, A.; Sougrati, M. T.; Grandjean, F.; Long, G. J.; Long, J. R.; Chang, C. J. *J. Am. Chem. Soc.* **2010**, *132*, 18115−18126.
(16) Zadrozny, J. M.; Atanasov, M.; Bryan, A. M.; Lin, C. Y.; Rekken, B. D.; Power, P. P.; Neese, F.; Long, J. R. *Chem. Sci.* **2013**, *4*, 125−138.
(17) Atanasov, M.; Zadrozny, J. M.; Long, J. R.; Neese, F. *Chem. Sci.* **2013**, *4*, 139−156.
(18) Freedman, D. E.; Harman, W. H.; Harris, T. D.; Long, G. J.; Chang, C. J.; Long, J. R. *J. Am. Chem. Soc.* **2010**, *132*, 1224−1225.
(19) Zadrozny, J. M.; Xiao, D. J.; Atanasov, M.; Long, G. J.; Grandjean, F.; Neese, F.; Long, J. R. *Nat. Chem.* **2013**, *5*, 577−581.
(20) Zadrozny, J. M.; Long, J. R. *J. Am. Chem. Soc.* **2011**, *133*, 20732−20734.
(21) Fukui, K.; Ohyanishiguchi, H.; Hirota, N. *Bull. Chem. Soc. Jpn.* **1991**, *64*, 1205−1212.
(22) Fukui, K.; Kojima, N.; Ohyanishiguchi, H.; Hirota, N. *Inorg. Chem.* **1992**, *31*, 1338−1344.
(23) Fukui, K.; Masuda, H.; Ohyanishiguchi, H.; Kamada, H. *Inorg. Chim. Acta* **1995**, *238*, 73−81.
(24) Fataftah, M. S.; Zadrozny, J. M.; Rogers, D. M.; Freedman, D. E. *Inorg. Chem.* **2014**, *53*, 10716−10721.
(25) Maganas, D.; Sottini, S.; Kyritsis, P.; Groenen, E. J. J.; Neese, F. *Inorg. Chem.* **2011**, *50*, 8741−8754.
(26) Saber, M. R.; Dunbar, K. R. *Chem. Commun.* **2014**, *50*, 12266−12269.
(27) Zadrozny, J. M.; Telser, J.; Long, J. R. *Polyhedron* **2013**, *64*, 209−217.
(28) Neese, F. *Wires Comput. Mol. Sci.* **2012**, *2*, 73−78.
(29) Neese, F.; with contributions from Becker, U.; Ganyushin, G.; Hansen, A.; Izsak, R.; Liakos, D. G.; Kollmar, C.; Kossmann, S.; Pantazis, D. A.; Petrenko, T.; Reimann, C.; Riplinger, C.; Roemelt, M.; Sandhöfer, B.; Schapiro, I.; Sivalingam, K.; Wennmohs, F.; Wezisla, B. and contributions from our collaborators: Kállay, M.; Grimme, S.; Valeev, E. *ORCA - An ab initio, DFT and semiempirical SCF-MO package*, Version 3.0; Max-Planck-Institute for Chemical Energy Conversion: Mülheim a. d. Ruhr, Germany. The binaries of ORCA are available free of charge for academic users for a variety of platforms.
(30) Becke, A. D. *Phys. Rev. A: At., Mol., Opt. Phys.* **1988**, *38*, 3098−3100.
(31) Perdew, J. P. *Phys. Rev. B: Condens. Matter Mater. Phys.* **1986**, *33*, 8822−8824.
(32) Schäfer, A.; Huber, C.; Ahlrichs, R. *J. Chem. Phys.* **1994**, *100*, 5829−5835.
(33) Weigend, F.; Ahlrichs, R. *Phys. Chem. Chem. Phys.* **2005**, *7*, 3297−3305.
(34) Schäfer, A.; Horn, H.; Ahlrichs, R. *J. Chem. Phys.* **1992**, *97*, 2571−2577.
(35) Grimme, S.; Antony, J.; Ehrlich, S.; Krieg, H. *J. Chem. Phys.* **2010**, *132*, 154104.
(36) Grimme, S.; Ehrlich, S.; Goerigk, L. *J. Comput. Chem.* **2011**, *32*, 1456−1465.
(37) Neese, F. *J. Comput. Chem.* **2003**, *24*, 1740−1747.
(38) Roos, B. O.; Taylor, P. R.; Siegbahn, P. E. M. *Chem. Phys.* **1980**, *48*, 157−173.
(39) Siegbahn, P.; Heiberg, A.; Roos, B.; Levy, B. *Phys. Scr.* **1980**, *21*, 323−327.
(40) Siegbahn, P. E. M.; Almlof, J.; Heiberg, A.; Roos, B. O. *J. Chem. Phys.* **1981**, *74*, 2384−2396.
(41) Angeli, C.; Cimiraglia, R.; Evangelisti, S.; Leininger, T.; Malrieu, J.-P. *J. Chem. Phys.* **2001**, *114*, 10252−10264.
(42) Angeli, C.; Cimiraglia, R.; Malrieu, J.-P. *Chem. Phys. Lett.* **2001**, *350*, 297−305.
(43) Angeli, C.; Cimiraglia, R. *Theor. Chem. Acc.* **2002**, *107*, 313−317.
(44) Angeli, C.; Cimiraglia, R.; Malrieu, J.-P. *J. Chem. Phys.* **2002**, *117*, 9138−9153.
(45) Neese, F. *J. Chem. Phys.* **2003**, *119*, 9428−9443.
(46) Hess, B. A. *Phys. Rev. A: At., Mol., Opt. Phys.* **1986**, *33*, 3742−3748.
(47) Pantazis, D. A.; Chen, X. Y.; Landis, C. R.; Neese, F. *J. Chem. Theory Comput.* **2008**, *4*, 908−919.
(48) Atanasov, M.; Ganyushin, D.; Sivalingam, K.; Neese, F. *Struct. Bonding (Berlin, Ger.)* **2011**, *143*, 149−220.
(49) Ganyushin, D.; Neese, F. *J. Chem. Phys.* **2013**, *138*, 104113.
(50) Vallet, V.; Maron, L.; Teichteil, C.; Flament, J.-P. *J. Chem. Phys.* **2000**, *113*, 1391−1402.
(51) Maurice, R.; Bastardis, R.; Graaf, C. d.; Suaud, N.; Mallah, T.; Guihéry, N. *J. Chem. Theory Comput.* **2009**, *5*, 2977−2984.
(52) Atanasov, M.; Ganyushin, D.; Pantazis, D. A.; Sivalingam, K.; Neese, F. *Inorg. Chem.* **2011**, *50*, 7460−7477.
(53) Holah, D. G.; Coucouvanis, D. *J. Am. Chem. Soc.* **1975**, *97*, 6917−6919.
(54) In usual considerations of cubic ligand fields of $d^{3,7}$ and $d^{2,8}$ complexes (all characterized by A_2 and T_2 ground state and first excited state, respectively, of the same spin) and their origin, $10Dq$ is being identified with the difference between the energies of the many

DOI: 10.1021/acs.inorgchem.5b01706
Inorg. Chem. 2015, 54, 9948−9961

electron $^4A_2$ and $^4T_2$ terms; see Gerloch,M.; Slade, R. C. *Ligand Field Parameters*; Cambridge University Press: Cambridge, 1973, and references therein. For the sake of analysis, we employ in the present study a definition of 10*Dq* based on ligand field orbitals, which also allows a direct link with the nature of the metal−ligand bond.
(55) Deeth, R. J.; Duer, M. J.; Gerloch, M. *Inorg. Chem.* **1987**, *26*, 2578−2582.
(56) Liehr, A. D. *J. Phys. Chem.* **1964**, *68*, 665−722.
(57) Gerloch, M.; Woolley, R. *Prog. Inorg. Chem.* **1984**, *31*, 371−446.
(58) Bridgeman, A. J.; Gerloch, M. The interpretation of ligand field parameters. In *Progress in Inorganic Chemistry*; Karlin, K. D., Ed.; John Wiley & Sons, Inc.: Hoboken, NJ, USA, 1996; Vol. *45*, pp 179−281.
(59) Jørgensen, C. K. Recent progress in ligand field theory. In *Structure and Bonding*; Springer: Berlin Heidelberg, 1966; Vol. *1*, pp 3−31.
(60) Bhattacharjee, A.; Chavarot-Kerlidou, M.; Dempsey, J. L.; Gray, H. B.; Fujita, E.; Muckerman, J. T.; Fontecave, M.; Artero, V.; Arantes, G. M.; Field, M. J. *ChemPhysChem* **2014**, *15*, 2951−2958.
(61) Bane, K.; Geiger, R. A.; Chabolla, S. A.; Jackson, T. A. *Inorg. Chim. Acta* **2012**, *380*, 135−140.
(62) Atanasov, M.; Aravena, D.; Suturina, E.; Bill, E.; Maganas, D.; Neese, F. *Coord. Chem. Rev.* **2015**, *289*, 177−214.
(63) White, R. M. *Quantum Theory of Magnetism: Magnetic Properties of Materials*; Springer: New York, 2007.
(64) Bain, G. A.; Berry, J. F. *J. Chem. Educ.* **2008**, *85*, 532.
(65) Kahn, O. *Molecular Magnetism*; Wiley: New York, 1993.
(66) Fujikawa, Y.; Fukui, M. *J. Contam. Hydrol.* **1991**, *8*, 177−195.
(67) Gebhard, M. S.; Koch, S. A.; Millar, M.; Devlin, F. J.; Stephens, P. J.; Solomon, E. I. *J. Am. Chem. Soc.* **1991**, *113*, 1640−1649.
(68) Vrajmasu, V. V.; Münck, E.; Bominaar, E. L. *Inorg. Chem.* **2004**, *43*, 4867−4879.

DOI: 10.1021/acs.inorgchem.5b01706
Inorg. Chem. 2015, 54, 9948−9961